Results on charmonium(-like) states from Belle

V. Zhukova
Belle Collaboration

"Quarkonium Working Group", Beijing, 6-10 November 2017

New measurement and angular analysis of the $e^+e^- \to D^{(*)+}D^{*-}$ process near the open charm threshold with initial state radiation

Spectrum of charmonium

- Vector states above open-charm threshold are not fully understood
- Parameters of ψ states obtained from $\sigma_{\text{tot}}(e^+e^- \to \text{hadrons})$
  - are model-dependent
  - have large uncertainties
- Data collected should allow for coupled-channel analysis

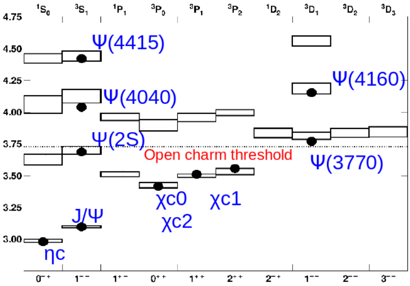

Spectrum of charmonium

- Vector states above open-charm threshold are not fully understood
- Parameters of ψ states obtained from $\sigma_{\text{tot}}(e^+e^- \to \text{hadrons})$
  - are model-dependent
  - have large uncertainties
- Data collected should allow for coupled-channel analysis

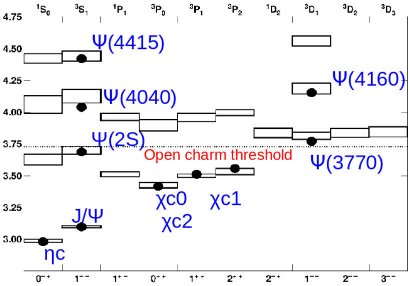

Solution $\Longrightarrow$ Measure exclusive cross sections

Comparison with previous results

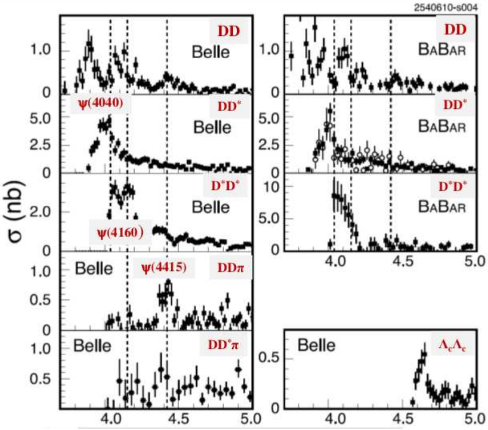

- Belle and BaBar results agree with each other
- Statistics is too low to study the structure of the cross sections
- Sum of all measured excusive cross-section to open-charm channels saturates the total cross section

Comparison with previous results

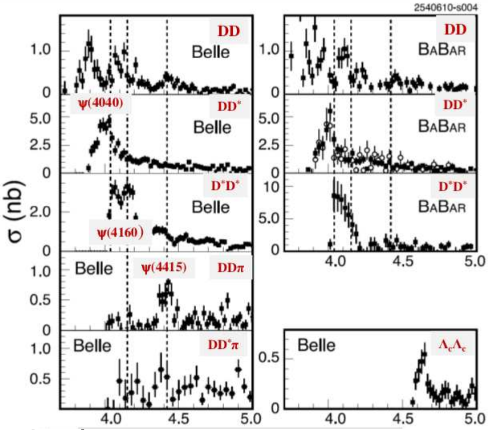

- Belle and BaBar results agree with each other
- Statistics is too low to study the structure of the cross sections
- Sum of all measured excusive cross-section to open-charm channels saturates the total cross section

Goals:

- To improve accuracy of cross section measurements
- To measure separately cross sections for all 3 possible helicity combinations (TT, LT, LL) for the $D^*\bar{D}^*$ final state

Method

- Partial reconstruction
- Reconstruct $\mathbf{D}^*$, γ_{ISR}

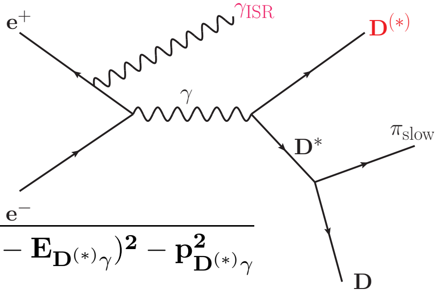

$$\mathbf{M}_{\mathsf{recoil}}(\mathbf{D}^{(*)}\gamma) = \sqrt{(\mathbf{E_{c.m.}} - \mathbf{E}_{\mathbf{D}^{(*)}\gamma})^2 - \mathbf{p}^2_{\mathbf{D}^{(*)}\gamma}}$$

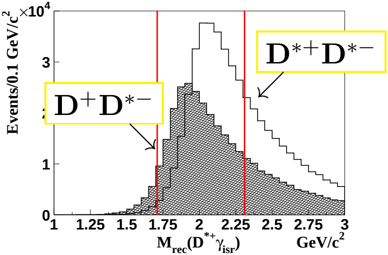

Method

- Partial reconstruction
- Reconstruct $\mathbf{D}^*$, γ_{ISR}

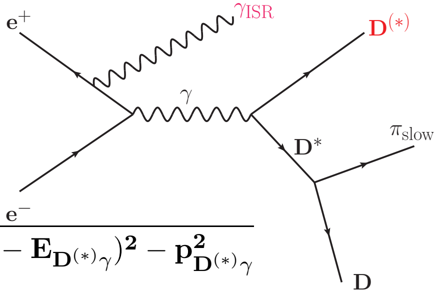

$$\mathbf{M}_{\mathsf{recoil}}(\mathbf{D}^{(*)}\gamma) = \sqrt{(\mathbf{E}_{\mathbf{c.m.}} - \mathbf{E}_{\mathbf{D}^{(*)}\gamma})^2 - \mathbf{p}^2_{\mathbf{D}^{(*)}\gamma}}$$

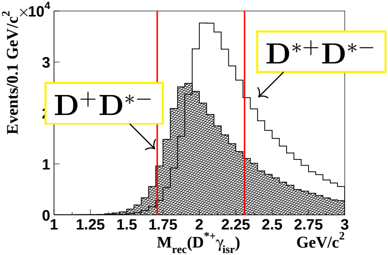

Problem: Cannot distinguish between $\mathbf{D}$, $\mathbf{D}^*$ and $\mathbf{D}^{**}$ in the final state

Method

- Partial reconstruction
- Reconstruct $\mathbf{D}^*$, γ_{ISR} and $\pi_{\mathbf{slow}}$

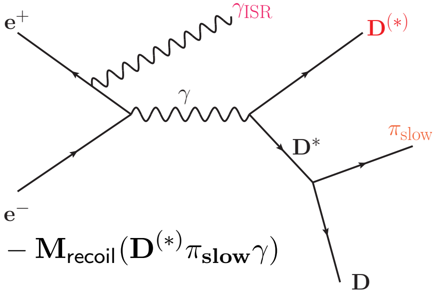

$$\Delta \mathbf{M}_{\text{recoil}} = \mathbf{M}_{\text{recoil}}(\mathbf{D}^{(*)}\gamma_{\text{ISR}}) - \mathbf{M}_{\text{recoil}}(\mathbf{D}^{(*)}\pi_{\mathbf{slow}}\gamma)$$

$\mathbf{e^+e^- \to D^+D^{*-}}$

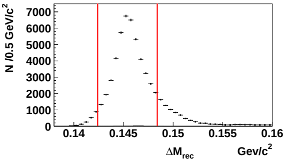

Recoil mass difference $\Delta \mathbf{M}_{\text{recoil}}$

↙ ↘

cut:

$\pm 3MeV/c^2$

$\mathbf{e^+e^- \to D^{*+}D^{*-}}$

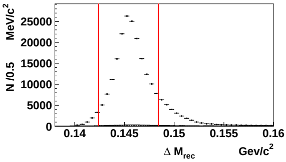

Method

- Partial reconstruction
- Reconstruct $\mathbf{D}^*$, γ_{ISR} and $\pi_{\mathbf{slow}}$
- $\mathbf{M}(\mathbf{D}^{(*)+}\mathbf{D}^{*-}) \equiv \mathbf{M}_{\text{recoil}}(\gamma_{\text{ISR}})$

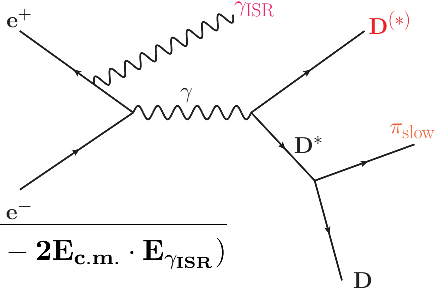

$$\mathbf{M}_{\text{recoil}}(\gamma_{\text{ISR}}) = \sqrt{(\mathbf{E}^2_{\mathbf{c.m.}} - \mathbf{2E}_{\mathbf{c.m.}} \cdot \mathbf{E}_{\gamma_{\mathbf{ISR}}})}$$

Refit $M_{\text{recoil}}(D^{(*)}\gamma_{\text{ISR}})$ to D^* mass to improve the $M_{\text{recoil}}(\gamma_{\text{ISR}})$ resolution

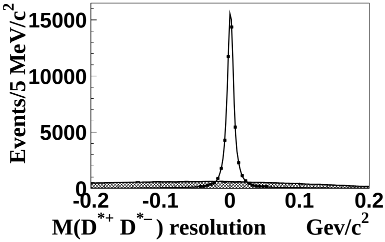

$\mathbf{M}_{\text{recoil}}(\gamma_{\text{ISR}})$ resolution:

Before re-fit — hatched histogram

After re-fit — solid line

Comparison with previous analysis

- Increased data sample: 547 fb^{-1} $\Longrightarrow$ 951 fb^{-1}

- Additional modes for D reconstruction $\Longrightarrow$ $\mathbf{D^0}$ decay channels:
  1. $K^-\pi^+$
  2. K^-K^+
  3. $K^-\pi^-\pi^+\pi^+$
  4. $K^0_S\pi^+\pi^-$
  5. $K^-\pi^+\pi^0$
  6. $K^0_S K^+ K^-$
  7. $K^0_S\pi^0$
  8. $K^-K^+\pi^-\pi^+$
  9. $K^0_S\pi^+\pi^-\pi^0$

- Extended signal region for $M_{\text{recoil}}(D^{(*)}\gamma_{\text{ISR}})$

$$|(M_{\text{recoil}}(D^{(*)+}\gamma_{\text{ISR}}) - M(D^{*-}))| < \not{200}\ 300 \ \text{MeV}/c^2$$

- $\sigma[e^+e^- \to D^{(*)+}D^{*-}] = \dfrac{dN/dM}{\eta_{\text{tot}}(M)\cdot dL/dM}$

dL/dM up to second-order QED corrections

(Kuraev & Fadin (1985))

Backgrounds

1. Combinatorial background under the reconstructed $D^{(*)+}$ peak
2. Real $D^{(*)+}$ mesons and a combinatorial π_{slow}
3. Both the $D^{(*)+}$ meson and π_{slow} are combinatorial
4. Reflections from the processes $e^+e^- \to D^{(*)+}D^{*-}\pi^0\gamma_{\text{ISR}}$ where the π^0 is lost
5. Contribution of the $e^+e^- \to D^{(*)+}D^{*-}\pi^0_{\text{fast}}$ where the hard π^0_{fast} is misidentified as γ_{ISR}

Background contribution estimated from the data

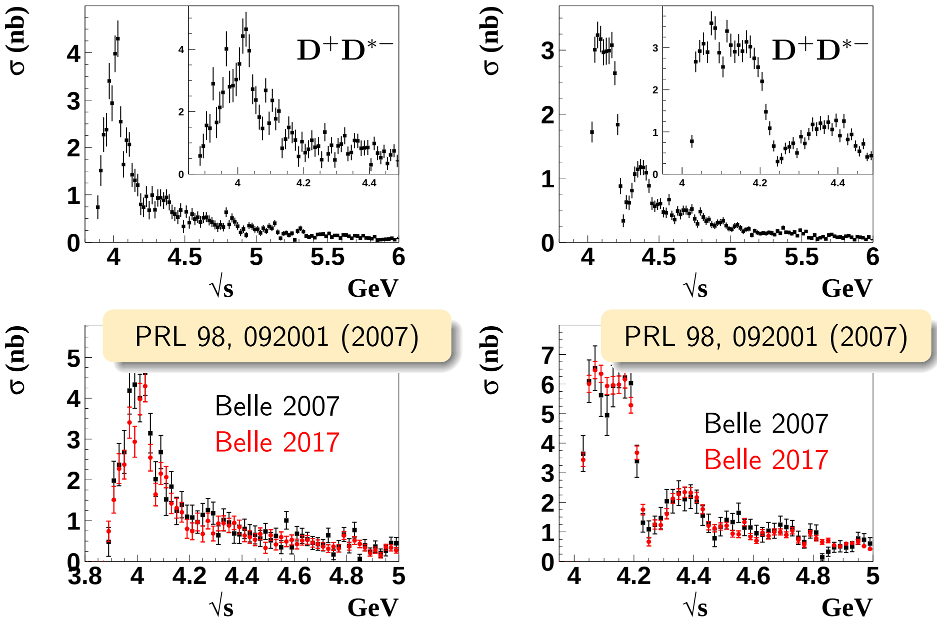
σ (nb)
D⁺D*⁻
√s
GeV
σ (nb)
D⁺D*⁻
√s
GeV
PRL 98, 092001 (2007)
σ (nb)
Belle 2007
Belle 2017
√s
GeV
PRL 98, 092001 (2007)
σ (nb)
Belle 2007
Belle 2017
√s
GeV

Angular analysis of the process $e^+e^- \to D^+D^{*-}$

- Study D^* helicity angle distribution in each bin of $M(D^+D^{*-})$
- D^* are transversely polarized
  $\Longrightarrow$ Check method

$$4.05 < M(D^+D^{*-}) < 4.3\mathrm{GeV}/c^2$$

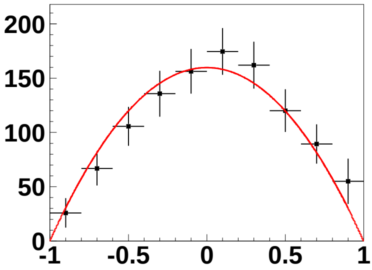

$$F(\cos\theta) = \eta(\cos\theta)\cdot dM/dL\cdot(f_L + f_T)$$

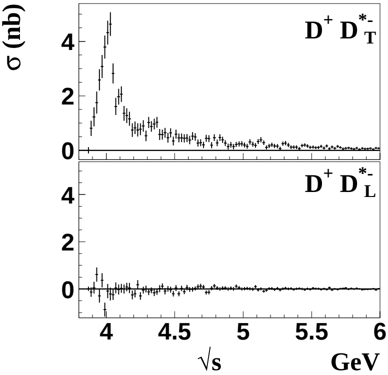

$$f_L = \sigma_L \cdot \cos^2\theta$$
$$f_T = \sigma_T \cdot (1 - \cos^2\theta)$$

Angular analysis of the process $\mathrm{e^+e^-} \to \mathbf{D^{*+}D^{*-}}$

- Study of the D^* helicity angle distribution in each bin of $M(D^{*+}D^{*-})$
- Helicity composition of the $D^{*+}D^{*-}$ final state:

$$\mathbf{D_T^{*+}D_T^{*-}},\ \mathbf{D_T^{*+}D_L^{*-}}\ \text{and}\ \mathbf{D_L^{*+}D_L^{*-}}$$

  - $D^*_{\mathrm{T}} \equiv$ transversely polarized D^* meson
  - $D^*_{\mathrm{L}} \equiv$ longitudinally polarized D^* meson
- Total cross section

$$\sigma = \sigma_{\mathrm{TT}} + \sigma_{\mathrm{TL}} + \sigma_{\mathrm{LL}}$$

$$f = \eta(c_1, c_2) \cdot dL/dM \cdot (f_{LL} + f_{TL} + f_{TT}) + f_{\mathrm{bg}}$$

$$c_1 \equiv \cos\theta_f \qquad c_2 \equiv \cos\theta_p$$

θ's are D^*'s helicity angles

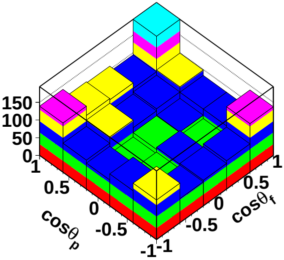

$$\begin{aligned} f_{TT} &= \sigma_{TT} \cdot (1 - c_1^2) \cdot (1 - c_2^2) \\ f_{TL} &= \sigma_{TL} \cdot \left((1 - c_1^2) \cdot c_2^2 + c_1^2 \cdot (1 - c_2^2)\right) \\ f_{LL} &= \sigma_{LL} \cdot c_1^2 \cdot c_2^2 \end{aligned}$$

Fit results

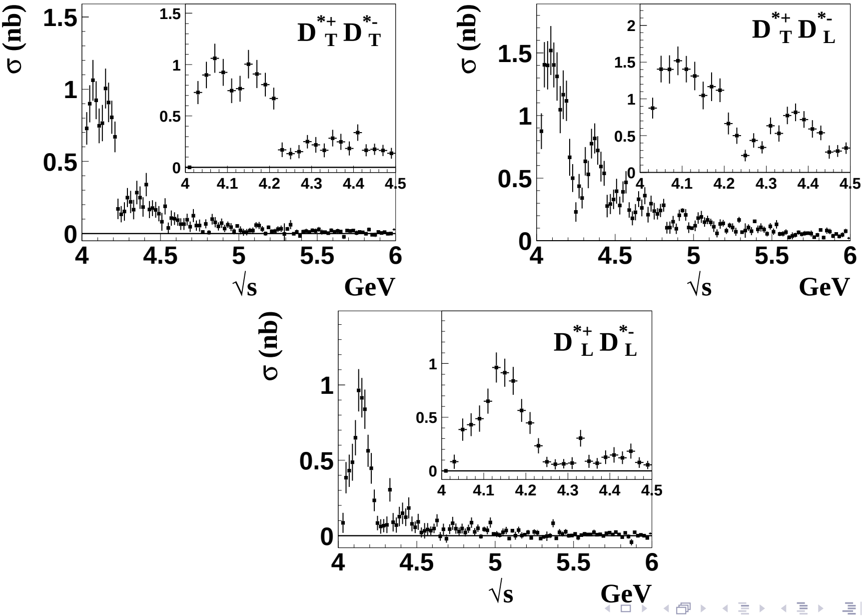

Conclusions

- We measured the exclusive cross sections of the $e^+e^- \to D^+D^{*-}$ and $e^+e^- \to D^{*+}D^{*-}$ processes
- The accuracy of the cross section measurements is increased
- The systematic uncertainties are significantly reduced
- For the $e^+e^- \to D^{*+}D^{*-}$ process we measured separately the cross sections for all three possible helicity final states (TT, LT and LL)

Observation of an alternative $\chi_{c0}(2P)$ candidate in $e^+e^- \to J/\psi D\bar{D}$

Motivation

$X(3915)$ ↗ Observed by Belle, confirmed by BaBar in $B \to (J/\psi\,\omega)K$

PRL **94**, 182002 (2005), PRD **82**, 011101 (2010)

$X(3915)$ ↘ Observed by both Belle and BaBar in $\gamma\gamma \to J/\psi\,\omega$

PRL **104**, 092001 (2010), PRD **86**, 072002 (2012)

BaBar: $J^P = 0^+ \Longrightarrow \chi_{c0}(2P)$ candidate

PRD **86**, 072002(2012)

Difficulties (see, *e.g.*, S. L. Olsen (2015), F.-K.Guo *et al.* (2012)):

- Too narrow: 20 MeV (measured) versus ∼100 MeV (expected)
- Not seen in $D\bar{D}$ (expected as dominating mode!)
- Unnaturally small 2^3P_2-2^3P_1 mass splitting
- Strong OZI violation: large BF in OZI-suppressed $J/\psi\,\omega$ mode

Motivation

$X(3915)$ ↗ Observed by Belle, confirmed by BaBar in $B \to (J/\psi\,\omega)K$

PRL **94**, 182002 (2005), PRD **82**, 011101 (2010)

$X(3915)$ ↘ Observed by both Belle and BaBar in $\gamma\gamma \to J/\psi\,\omega$

PRL **104**, 092001 (2010), PRD **86**, 072002 (2012)

BaBar: $J^P = 0^+ \implies \chi_{c0}(2P)$ candidate

PRD **86**, 072002(2012)

Difficulties (see, *e.g.*, S. L. Olsen (2015), F.-K.Guo *et al.* (2012)):

- Too narrow: 20 MeV (measured) versus ∼100 MeV (expected)
- Not seen in $D\bar{D}$ (expected as dominating mode!)
- Unnaturally small 2^3P_2-2^3P_1 mass splitting
- Strong OZI violation: large BF in OZI-suppressed $J/\psi\,\omega$ mode

Search for alternative $\chi_{c0}(2P)$ candidate in $e^+e^- \to J/\psi D\bar{D}$ annihilation

Method

$$e^+e^- \to J/\psi D\bar{D}, \qquad D \equiv D^0 \text{ or } D^+$$

$$\mathbf{M}_{\mathrm{rec}}(\mathbf{J}/\psi, \mathbf{D}) = \sqrt{(\mathbf{p}_{\mathrm{e^+e^-}} - \mathbf{p}_{\mathrm{J}/\psi} - \mathbf{p}_{\mathrm{D}})^2}$$

- $J/\psi \to \{e^+e^-, \mu^+\mu^-\}$
- Both D^0 and D^+ used:
  - $D^0 \to \{K^-\pi^+, K_s^0\pi^+\pi^-, K^-\pi^+\pi^0, K^-\pi^+\pi^+\pi^-\}$ (4 channels)
  - $D^+ \to \{K_s^0\pi^+, K^-\pi^+\pi^+, K_s^0\pi^+\pi^0, K^-\pi^+\pi^+\pi^0, K_s^0\pi^+\pi^+\pi^-\}$ (5 channels)
- Signal and background separated using the MLP neural network
- Global optimization of the selection requirements: 4 variables per D channel (signal regions in $M_{J/\psi}$, M_D, $M_{\mathrm{rec}}(J/\psi, D)$ and MLP output cutoff value)

Resulting sample: 103 events with $24.9 \pm 1.1 \pm 1.6$ background events

Signal fit

Amplitude analysis in 6D phase space: $\{M_{D\bar{D}},\ \theta_{\text{prod}},\ \theta_{\text{J}/\psi},\ \theta_{\text{X}^*},\ \phi_{\text{l}^-},\ \phi_{\text{D}}\}$

$$S(\Phi) = \sum_{\substack{\lambda_{\text{beam}}=-1,1 \\ \lambda_{\ell\ell}=-1,1}} \left| \sum_{X^*} A_{\lambda_{\text{beam}}\,\lambda_{\ell\ell}}(\Phi) A_{X^*}(M_{D\bar{D}}) \right|^2$$

Resonance: A_{X^*} — relativistic BW,

Non-resonant amplitude:

$A_{X^*} = \sqrt{F_{D\bar{D}}(M_{D\bar{D}})}$,

$F_{D\bar{D}}(M_{D\bar{D}})$ - non-resonant form factor,

default model: $F_{D\bar{D}} = 1$

Model: X^* + non-resonant contribution

J^{PC}	Mass, MeV/c^2	Width, MeV	Significance
0^{++}	3862^{+26}_{-32}	201^{+154}_{-67}	9.1σ
2^{++}	3879^{+20}_{-17}	171^{+129}_{-62}	8.0σ
2^{++}	3879^{+17}_{-17}	148^{+108}_{-50}	8.0σ
2^{++}	3883^{+26}_{-24}	227^{+201}_{-125}	8.0σ

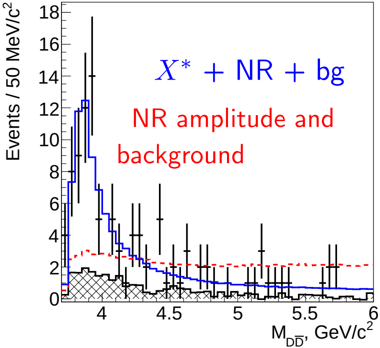

$J^{PC} = 0^{++}$ versus $J^{PC} = 2^{++}$

Approach: Toy MC pseudoexperiments generated in accordance with fit results for $J^{PC} = 0^{++}$ and 2^{++} and fitted for both hypotheses

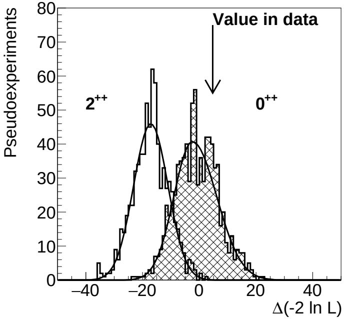

Result:

- $J^{PC} = 2^{++}$ excluded at the level 2.5σ including systematics
- $J^{PC} = 0^{++}$ with CL=77% (default model)

$X^*(3860)$ versus $X(3915)$ — the fight for $\chi_{c0}(2P)$

	Theory	$X(3915)$	$X^*(3860)$
J^{PC}	0^{++}	$\pm$	$+$
Mass	3854 MeV/c^2 (Ebert *et al.*) 3916 MeV/c^2 (Godfrey *et al.*)	$\pm$	$+$
Width	Broad ($\Gamma \sim 100$ MeV)	$-$	$+$
$\frac{m_{\chi_{c2}(2P)}-m_{\chi_{c0}(2P)}}{m_{\chi_{c2}(1P)}-m_{\chi_{c0}(1P)}}$	$0.6..0.9$	$-$	$+$
BF($D\bar{D}$)	Large	$-$	$+$
BF($J/\psi\,\omega$)	Small	$-$	$+$

In addition, $X^*(3860)$

- is produced similarly to $\chi_{c0}(1P)$ (Belle (2004))
- agrees with the peak in $\gamma\gamma$ data with $M = 3837.6 \pm 11.5$ MeV$/c^2$ and $\Gamma = 221 \pm 19$ MeV

$X^*(3860)$ versus $X(3915)$ — the fight for $\chi_{c0}(2P)$

	Theory	$X(3915)$	$X^*(3860)$
J^{PC}	0^{++}	$\pm$	$+$
Mass	3854 MeV$/c^2$ (Ebert *et al.*)		

Conclusion: $X^*(3860)$ wins!

BF(DD)	Large	$-$	$+$
BF$(J/\psi\,\omega)$	Small	$-$	$+$

In addition, $X^*(3860)$

- is produced similarly to $\chi_{c0}(1P)$ (Belle (2004))
- agrees with the peak in $\gamma\gamma$ data with $M = 3837.6 \pm 11.5$ MeV$/c^2$ and $\Gamma = 221 \pm 19$ MeV

Conclusions

- A new charmoniumlike state X(3860) is observed
- $M = 3862^{+26}_{-32}\,^{+40}_{-13}$ MeV/c^2
- $\Gamma = 201^{+154}_{-67}\,^{+88}_{-82}$ MeV
- $J^{PC} = 0^{++}$ favoured

X(3860) $\Longrightarrow$ good $\chi_{c0}(2P)$ candidate

Conclusions

- A new charmoniumlike state X(3860) is observed
- $M = 3862^{+26}_{-32}\,{}^{+40}_{-13}\,\text{MeV}/c^2$
- $\Gamma = 201^{+154}_{-67}\,{}^{+88}_{-82}\,\text{MeV}$
- $J^{PC} = 0^{++}$ favoured

X(3860) $\Longrightarrow$ good $\chi_{c0}(2P)$ candidate

Thank you for your attention!

Criteria

- $|dr| < 2\,\mathrm{cm}$ and $|dz| < 4\,\mathrm{cm}$
- $\mathcal{P}_{K/\pi} = \mathcal{L}_K/(\mathcal{L}_K + \mathcal{L}_\pi) > 0.6$

$\mathbf{K_S}$ candidates:

- $|M_{inv}(\pi^+\pi^-) - M_{K_S^0}| < 15$ MeV/c^2
- the distance between the two pion tracks $< 1\,\mathrm{cm}$
- the transverse flight distance from IP $> 0.1\,\mathrm{cm}$
- the angle between the K_S momentum direction and decay path in $x - y$ plane $< 0.1\,\mathrm{rad}$

π_0 candidates:

- $|M_{inv}(\gamma\gamma) - M_{\pi_0}| < 15$ MeV/c^2

$\mathbf{D^0}$ decay channels:

1. $K^-\pi^+$
2. K^-K^+
3. $K^-\pi^-\pi^+\pi^+$
4. $K_S^0\pi^+\pi^-$
5. $K^-\pi^+\pi^0$
6. $K_S^0K^+K^-$
7. $K_S^0\pi^0$
8. $K^-K^+\pi^-\pi^+$
9. $K_S^0\pi^+\pi^-\pi^0$

$\mathbf{D^+}$ decay channels:

1. $K^+\pi^-\pi^-$
2. $K_S^0\pi^-$
3. $K_S^0K^+$

$\mathbf{D^*}$ decay channels:

1. $D^0\pi^+$

Analysis of the process $e^+e^- \to D^{(*)+}D^{*-}$

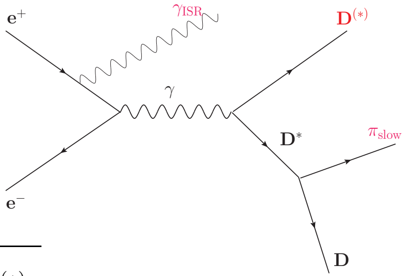

Method:

- partial reconstruction;
- reconstruction $\mathbf{D}^*$, $\pi_{\mathbf{slow}}$ and γ_{ISR};

$$M_{\text{recoil}}(D^{(*)}\gamma) = \sqrt{(E_{c.m.} - E_{D^{(*)}\gamma})^2 - p^2_{D^{(*)}\gamma}}$$

$$\Delta M_{\text{recoil}} = M_{\text{recoil}}(D^{(*)}\gamma_{\text{ISR}}) - M_{\text{recoil}}(D^{(*)}\pi_{slow}\gamma)$$

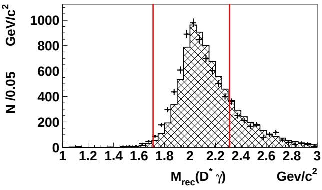

Spectrum of $M_{\text{recoil}}(D^*\gamma_{\text{ISR}})$

$$M_{\text{recoil}}(D^{(*)}\gamma) = \sqrt{(E_{c.m.} - E_{D^{(*)}\gamma})^2 - p^2_{D^{(*)}\gamma}}$$

Correction of γ_{ISR} energy

reference channel

$$e^+e^- \to \psi(2S)\gamma_{\text{ISR}}$$
$$\searrow$$
$$\psi(2S) \to J/\psi\pi^+\pi^-$$

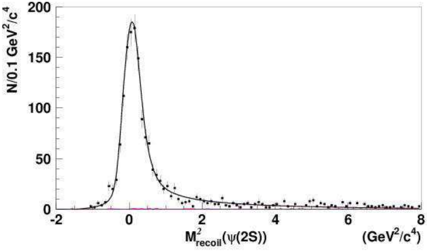

Conclusions:

phokhara generator describes the second radiation correction correctly

The same process on the other side

The recoil mass $\mathbf{M}_{\text{recoil}}(\mathbf{J}/\psi\pi^+\pi^-)$

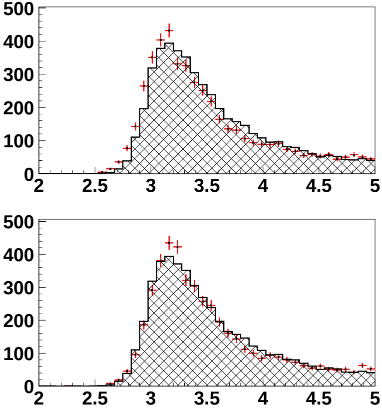

The recoil mass $M_{\text{recoil}}(D^* \gamma_{\text{ISR}})$

before correction γ_{ISR} energy

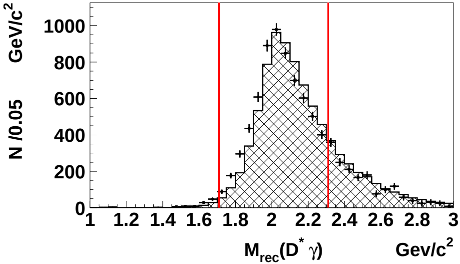

after correction γ_{ISR} energy

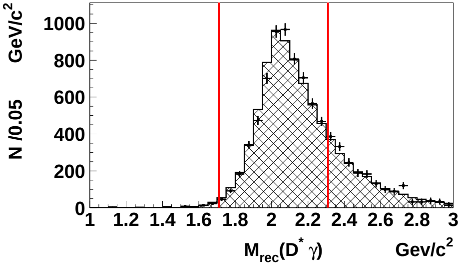

cut:

$$|M_{\text{recoil}}(D^* \gamma_{\text{ISR}}) - M(D^*)| < 300 MeV/c^2$$

Backgrounds

1. Combinatorial background under the reconstructed $D^{(*)+}$ peak
2. Real $D^{(*)+}$ mesons and a combinatorial π_{slow}
3. Both the $D^{(*)+}$ meson and π_{slow} are combinatorial
4. Reflections from the processes $e^+e^- \to D^{(*)+}D^{*-}\pi^0\gamma_{\text{ISR}}$ where the π^0 is lost
5. Contribution of the $e^+e^- \to D^{(*)+}D^{*-}\pi^0_{\text{fast}}$ where the hard π^0_{fast} is misidentified as γ_{ISR}

$e^+e^- \to D^+D^{*-}$

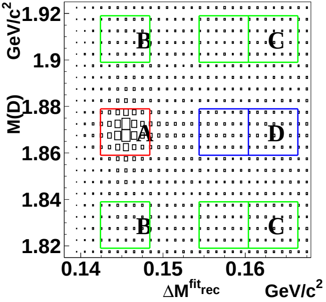

$e^+e^- \to D^{*+}D^{*-}$

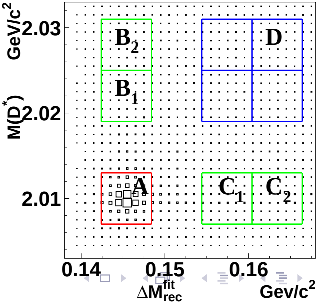

Mass spectra

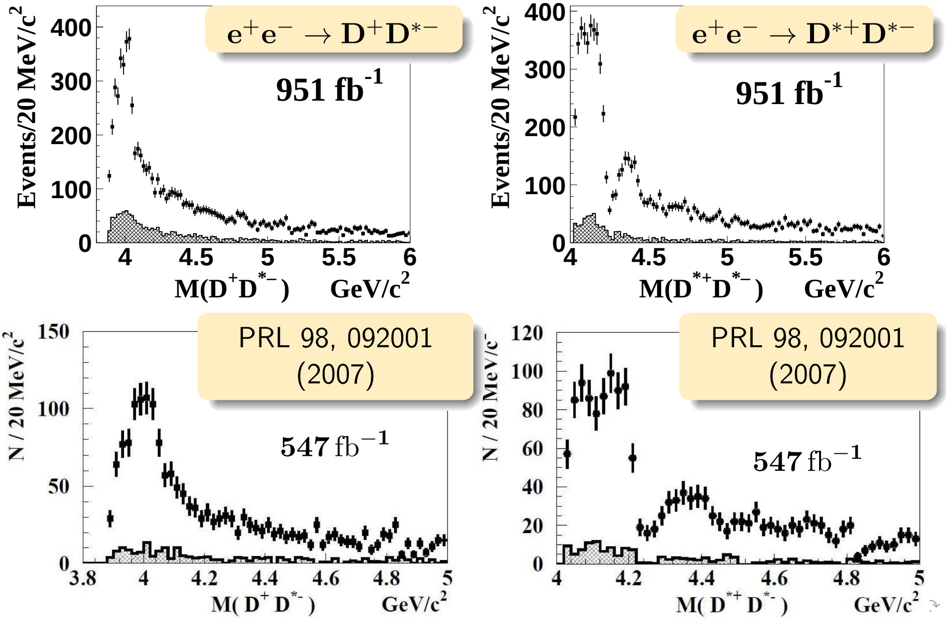

Reflection from the processes $e^+e^- \to D^{(*)+}D^{*-}\pi^0\gamma_{ISR}$

$e^+e^- \to D^+D^{*-}$ | $e^+e^- \to D^{*+}D^{*-}$

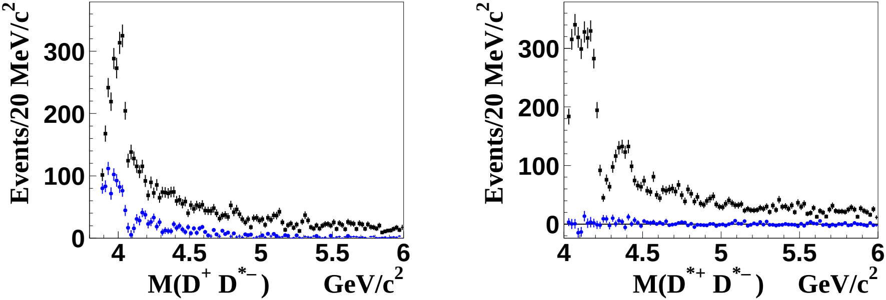

Background (blue points) from

$$e^+e^- \to D^{(*)+}D^{*-}\pi^0_{\text{miss}}\gamma_{\text{ISR}}$$

is evaluated from the isospin-conjugated process

$$e^+e^- \to D^{(*)0}D^{*-}\pi^+_{\text{miss}}\gamma_{\text{ISR}}$$

with the reconstruction of $D^{(*)0}$, π^-_{slow} and γ_{ISR}

Backgrounds

$$e^+e^- \to D^{*+}D^{*-}$$

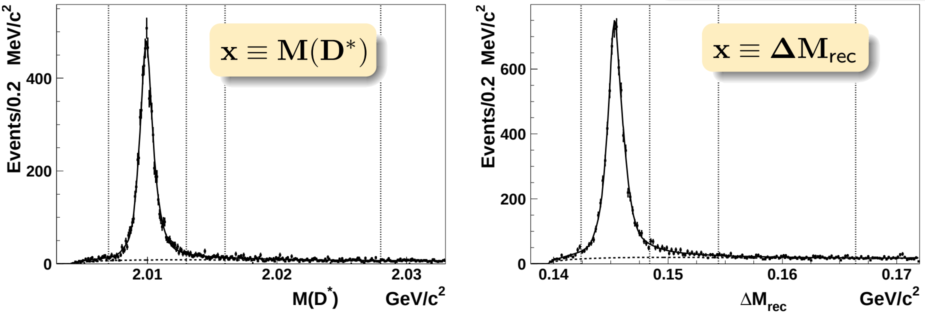

$$f = f_{\text{signal}} + f_{\text{background}}$$

$$f_{\text{background}} = \alpha \cdot \sqrt{x} \cdot (1 + \beta \cdot x + \gamma \cdot x^2)$$

$$M_{\text{bg (1)-(3)}} = 0.58 \cdot M_{\text{sb B}} + 0.53 \cdot M_{\text{sb C}} - 0.307 \cdot M_{\text{sb D}}$$

Backgrounds

$\mathbf{e^+e^- \to D^+D^{*-}}$

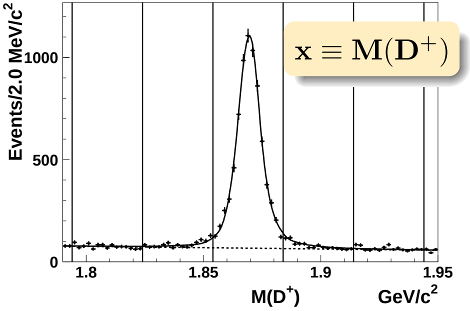

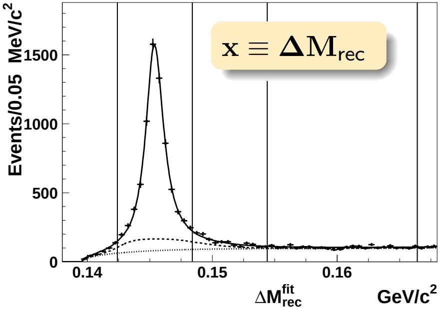

$$f = f_{\text{signal}} + f_{\text{background}}$$

$$f_{\text{background}} = \alpha \cdot \sqrt{x} \cdot (1 + \beta \cdot x + \gamma \cdot x^2)$$

$$M_{\text{bg (1)-(3)}} = 0.5 \cdot M_{\text{sb B}} + 0.5 \cdot M_{\text{sb C}} - 0.25 \cdot M_{\text{sb D}}$$

Cross sections calculation

$$e^+e^- \to D^+D^{*-}$$

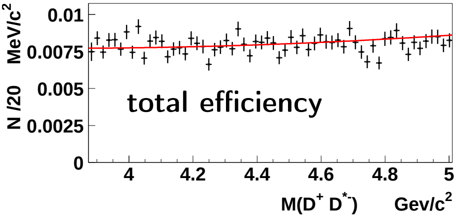

$$e^+e^- \to D^{*+}D^{*-}$$

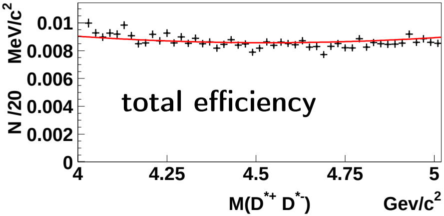

$$\sigma_{e^+e^-\to D^{(*)+}D^{*-}} = \frac{dN/dM}{\eta_{tot}(M)\cdot dL/dM}$$

dN/dM - mass spectrum,

η_{tot} - total efficiency,

dL/dM - differential luminosity;

$4.0 < M(D^{*+}D^{*-}) < 4.1\mathrm{GeV}/c^2$

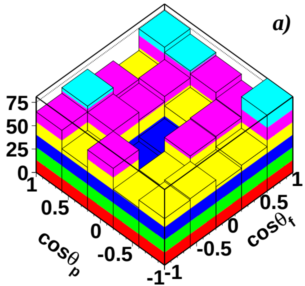

$4.1 < M(D^{*+}D^{*-}) < 4.25\mathrm{GeV}/c^2$

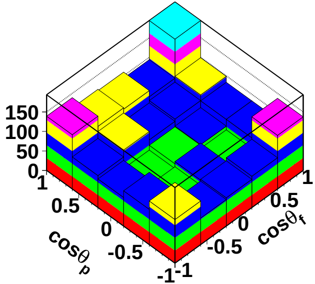

$4.25 < M(D^{*+}D^{*-}) < 4.6\mathrm{GeV}/c^2$

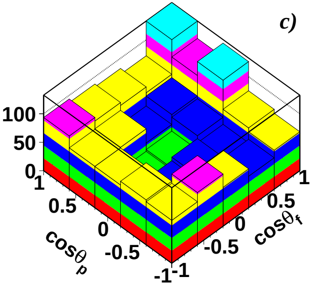

$M(D^{*+}D^{*-}) > 4.6\mathrm{GeV}/c^2$

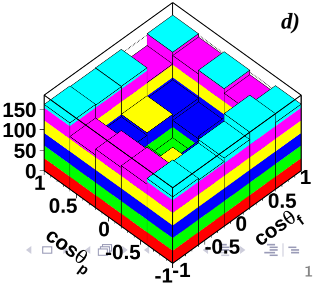

The summary of the systematic errors in the cross section calculation.

Source	D^+D^{*-}	$D^{*+}D^{*-}$
Background subtraction	2%	2%
Reconstruction	3%	4%
Selection	1%	1%
Angular distribution	–	2%
Cross section calculation	1.5%	1.5%
$\mathcal{B}(D^{(*)})$	2%	3%
MC statistics	1%	2%
Total	5%	7%

Signal fit

$$S(\Phi) = \sum_{\substack{\lambda_{\text{beam}}=-1,1 \\ \lambda_{\ell\ell}=-1,1}} \left| \sum_{X^*} A_{\lambda_{\text{beam}}\,\lambda_{\ell\ell}}(\Phi) A_{X^*}(M_{D\bar{D}}) \right|^2, \tag{1}$$

Here, $A_{\lambda_{\text{beam}}\,\lambda_{\ell\ell}}(\Phi)$ is the signal amplitude calculated using the helicity formalizm (the phase space Φ is 6-dimensional). For resonance, A_{X^*} = relativistic Breit-Wigner. For nonresonant amplitude, $A_{X^*} = \sqrt{F_{D\bar{D}}(M_{D\bar{D}})}$, where $F_{D\bar{D}}(M_{D\bar{D}})$ is the nonresonant amplitude form factor ($F_{D\bar{D}} = 1$ by default). Alternatives: mass dependence of NRQCD prediction for $e^+e^- \to \psi\chi_c$ [PRD **77**, 014002 (2008)], $F_{D\bar{D}} = M_{D\bar{D}}^{-4}$ [Victor Chernyak, based on PLB **612**, 215 (2005)].

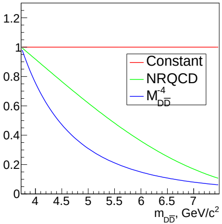

Signal fit results

Fit results in the default model. For the 2^{++} hypothesis, there are three solutions (fit is started 1000 times from random initial values in order to check for that).

J^{PC}	Mass, MeV/c^2	Width, MeV	Significance
0^{++}	3862^{+26}_{-32}	201^{+154}_{-67}	9.1σ
2^{++}	3879^{+20}_{-17}	171^{+129}_{-62}	8.0σ
2^{++}	3879^{+17}_{-17}	148^{+108}_{-50}	8.0σ
2^{++}	3883^{+26}_{-24}	227^{+201}_{-125}	8.0σ

Red dashed line - only background and nonresonant amplitudes, blue solid line - X^*, $J^{PC} = 0^{++}$.